

Thermally activated crystalline phase restoration in disordered barium ferrite powder prepared by ball milling

W. A. KACZMAREK, Z. L. LI

Institute of Advanced Studies, Department of Applied Mathematics, Research School of Physical Sciences and Engineering, The Australian National University, Canberra, ACT, 0200, Australia

Depending on milling conditions (air or vacuum) for the same milling time, a different level of decomposition and structure disorder in $\text{BaFe}_{12}\text{O}_{19}$ ferrite powders can be obtained by ball milling. Air-milled material has a tendency to form a gas-saturated disordered structure (superoxide) and to transform into simple oxides (reduction process through oxygen-saturated disordered phase) as opposed to the vacuum-milled powder where a highly disordered phase occurs. Both powders have a different morphology (particle size and distribution). Annealing processes produce crystalline barium ferrite phase with interesting magnetic properties, but in the present paper only structural transformations are analysed. Scanning electron microscopy, X-ray diffraction and thermal analysis techniques were applied to study the effects of heat treatment (10 h at 773 or 1273 K) in disordered $\text{BaFe}_{12}\text{O}_{19}$ ferrite powders prepared by 1000 h ball milling in air and vacuum.

1. Introduction

The influence of prolonged ball milling of $\text{BaFe}_{12}\text{O}_{19}$ ferrite powder on its structure and particle morphology was described in the parallel paper [1]. It was found there that mechanical processing in air promotes faster crystallographic structure disordering and final decomposition of the material into simple oxides, with haematite as a major component detectable by X-ray diffraction (XRD). A similar process performed over the same period of time in vacuum shows only structural disorder with similar magnetic characteristics as for pre-milled barium ferrite. Contrary to this, recently we found the opposite effect for haematite ($\alpha\text{-Fe}_2\text{O}_3$) milled in vacuum. A vacuum promotes a chemical reduction process and the $\alpha\text{-Fe}_2\text{O}_3$ fully transforms into magnetite (Fe_3O_4) powder [2]. Milling in air produces no structural changes and the haematite or magnetite powders are stable. This behaviour shows that at room temperature, chemical reduction is possible and it is only the value of partial oxygen pressure during milling that influences the final powder composition. By applying the same ideas to a complex oxide system for which barium ferrite is a typical example, the structure stability during milling was investigated. As mentioned above, the results are opposite in behaviour to that for the simple oxide.

In this work, in order to gain more insight into the process of thermally activated structure transformation from disordered to strongly ordered phases (this process will be called “phase restoration”) has been studied by XRD, thermogravimetric (TGA), differential scanning calorimetry (DSC) thermal analysis tech-

niques. Experiments performed on as-milled and annealed barium ferrite samples are discussed. Additionally, by using scanning electron microscopy (SEM) in parallel with the structure changes, we investigated the influence of heat treatment on the powder particle morphology in relation to preparation routes, i.e. powder obtained by ball milling in air and vacuum.

2. Experimental procedure

High-purity (99.99 wt %) barium ferrite powder ($\text{BaFe}_{12}\text{O}_{19}$) with particle size distribution in the 0.5–50 μm range (Alfa Products/Jonson Matthey) was used as a starting material. The X-ray powder diffraction pattern shows perfect hexagonal-type structure, characteristic for M-type ferrites (similar to magnetoplumbite mineral). Starting sample characterization and mechanical ball-milling preparation details were described extensively in the previous paper [1]. An additional two samples were obtained by milling in air and vacuum (10^2 – 10^3 Pa) for 1000 h, and will be denoted in this paper as A1000 and V1000 respectively. Heat treatment was performed on A1000 and V1000 powders at 773 and 1273 K in an air atmosphere and in vacuum (sealed quartz tube) for 4 h. The experiments then yielded: for air-milled material AA773, AA1273 (annealed in air) and AV773, AV1273 (annealed in vacuum) samples, and for vacuum-milled powder VA773, VA1273 (annealed in air) and VV773, VV1273 (annealed in vacuum), respectively. After milling and heat treatment, the morphology and structural analyses were performed. Particle morphology

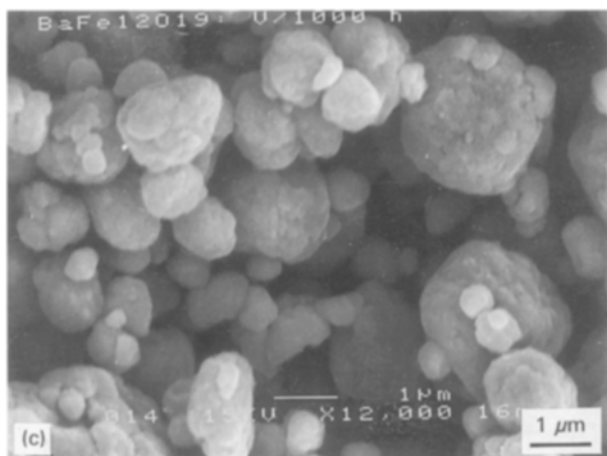
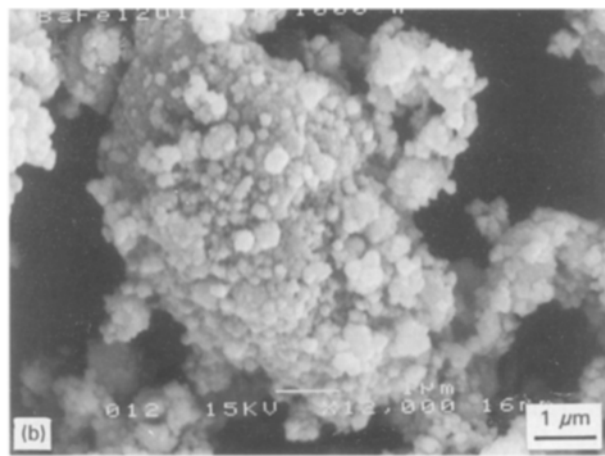
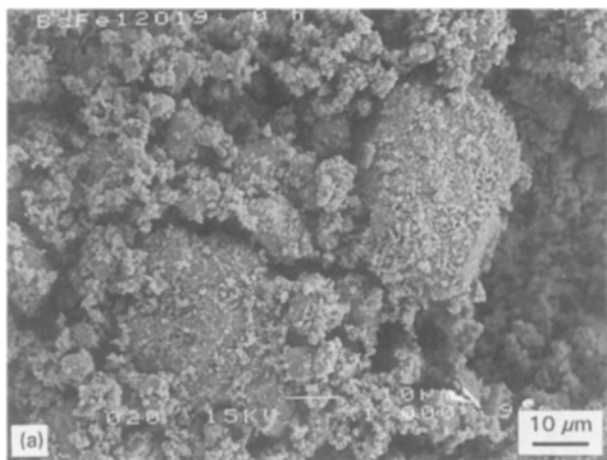


Figure 1 Scanning electron micrographs of $\text{BaFe}_{12}\text{O}_{19}$ powders: (a) pre-milled, (b) milled 1000 h in air, and (c) milled 1000 h in vacuum.

was examined by direct observation of gold-coated samples on a Jeol SEM 6400 scanning electron microscope. Structural characterization was performed using a Philips X-ray powder diffractometer employing CoK_α ($\lambda = 1.789 \text{ nm}$) radiation. The calorimetric and thermogravimetric experiments were performed in a Shimadzu DSC-50 and TGA-50H thermoanalysis system, on $\sim 20 \text{ mg}$ material under a dynamic pure argon atmosphere with a flow rate 50 ml min^{-1} . The temperature sweep rate was 15 K min^{-1} for DSC and 30 K min^{-1} for TGA.

3. Results and discussion

3.1. SEM analysis

3.1.1. Starting material

Scanning electron micrographs of pre-milled barium ferrite and powders obtained after 1000 h ball milling in air (A1000) as well as in vacuum (V1000) are shown in Fig. 1. The difference between powder particle morphology is clear. The broadest particle-size distribution, $0.5\text{--}50 \mu\text{m}$, can be found for pre-milled material. For the next two samples, it is obvious that milling increases particle size homogeneity. After milling for 1000 h, the particles processed in air are in the submicrometre range ($0.1\text{--}0.5 \mu\text{m}$), contrary to larger particles characteristic for powder milled in vacuum ($0.5\text{--}1.5 \mu\text{m}$). It was found that for air-milled powder (A1000), the particles have a tendency to agglomerate

with average clusters in the $5\text{--}10 \mu\text{m}$ size range. We note that formation of agglomerates in this powder has a physico-chemical origin, in which a surface gas layer (oxygen and nitrogen in air) plays the major role as a medium between fine particles. In surface-chemistry terms, this behaviour can be described as a result of weak intermolecular forces (attractive Van der Waals interaction) which causes the adherence of molecules on a surface and the agglomeration of small particles [3]. Any magnetic interaction between powder particles can be discounted because of the paramagnetic nature of air-milled material.

A different behaviour was observed for vacuum-milled barium ferrite powder. Instead of clusters of fine particles, a tendency to form a classical “mechanical alloying” product (larger compacted particles) can be noticed. We use the term “mechanical alloying” because of the similarity to the normally observed effect of milling of metal particles (soft material), wherein the smallest particles are welded together to form amorphous or polycrystalline larger particles (i.e. mechanically activated alloy formation). In this type of preparation, typically with increasing milling time, the particle size acquires a minimum and then the average size increases. This type of behaviour was observed and is characteristic for vacuum-milled barium ferrite powder (V1000), but not for the air-milled A1000 material described above.

3.1.2. Annealed powders

In Figs 2 and 3, scanning electron micrographs of A1000 and V1000 powders, annealed in air and vacuum, are shown. The photographs are grouped in two columns with a magnification of 5000 first and 20000 second; and two sections (a–d) showing powders annealed in air and (e–h) annealed in vacuum. From both Figs 2 and 3 the difference in particle morphology, which confirms the influence of air or vacuum during heat treatment, is visible. For A1000 powder annealed in air at 1273 K (sample AA1273), we found that a deagglomeration process is taking place, and after heat treatment all powder particles were found to be separated. For sample AA773

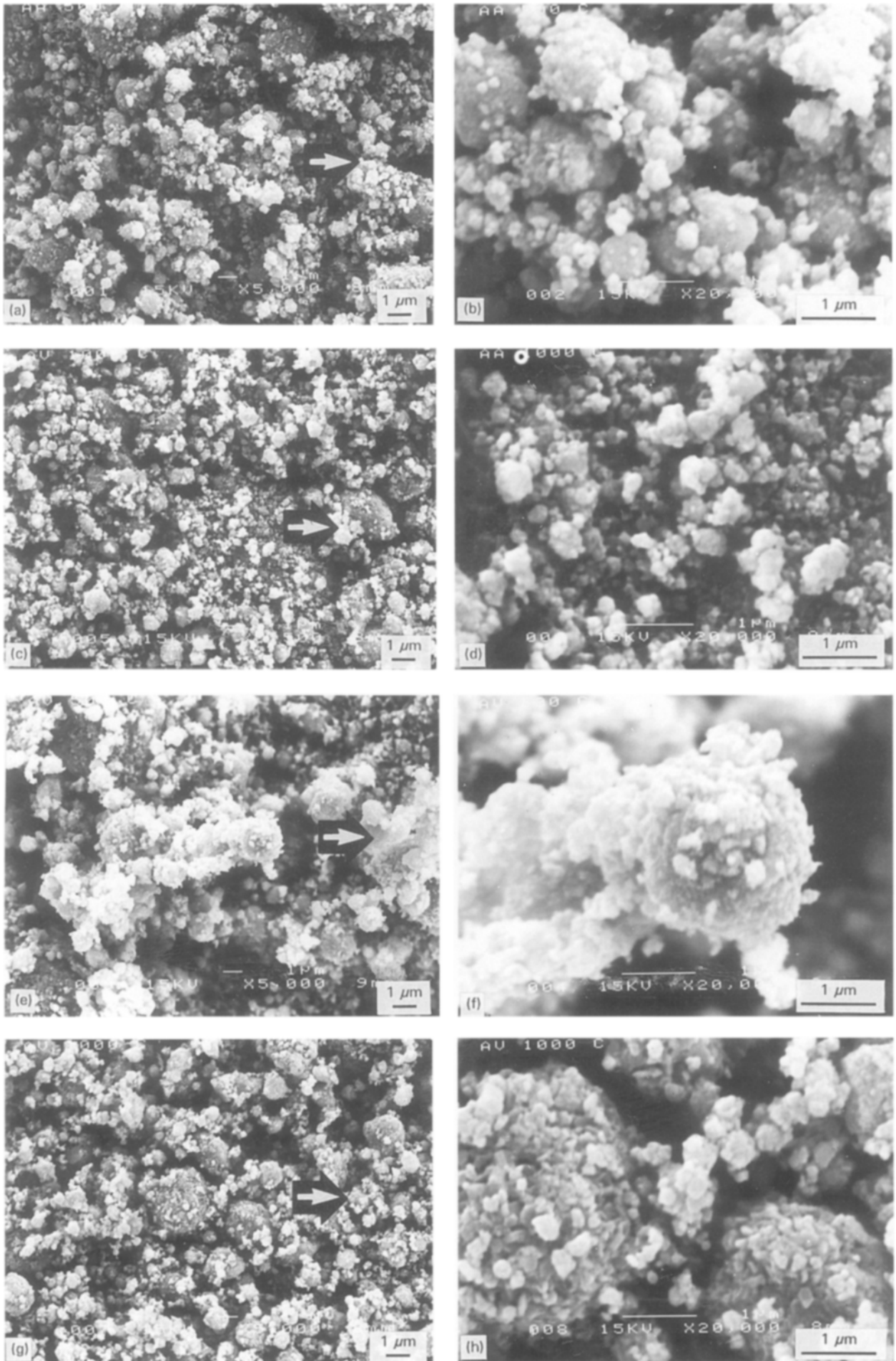


Figure 2 SEM analysis of air-milled barium ferrite powder versus annealing temperature ((a, b, e, f) 773 and (c, d, g, h) 1273 K) performed in air (A) and vacuum (V). (a, b) AA773, (c, d) AA1273, (e, f) AV773, (g, h) AV1273.

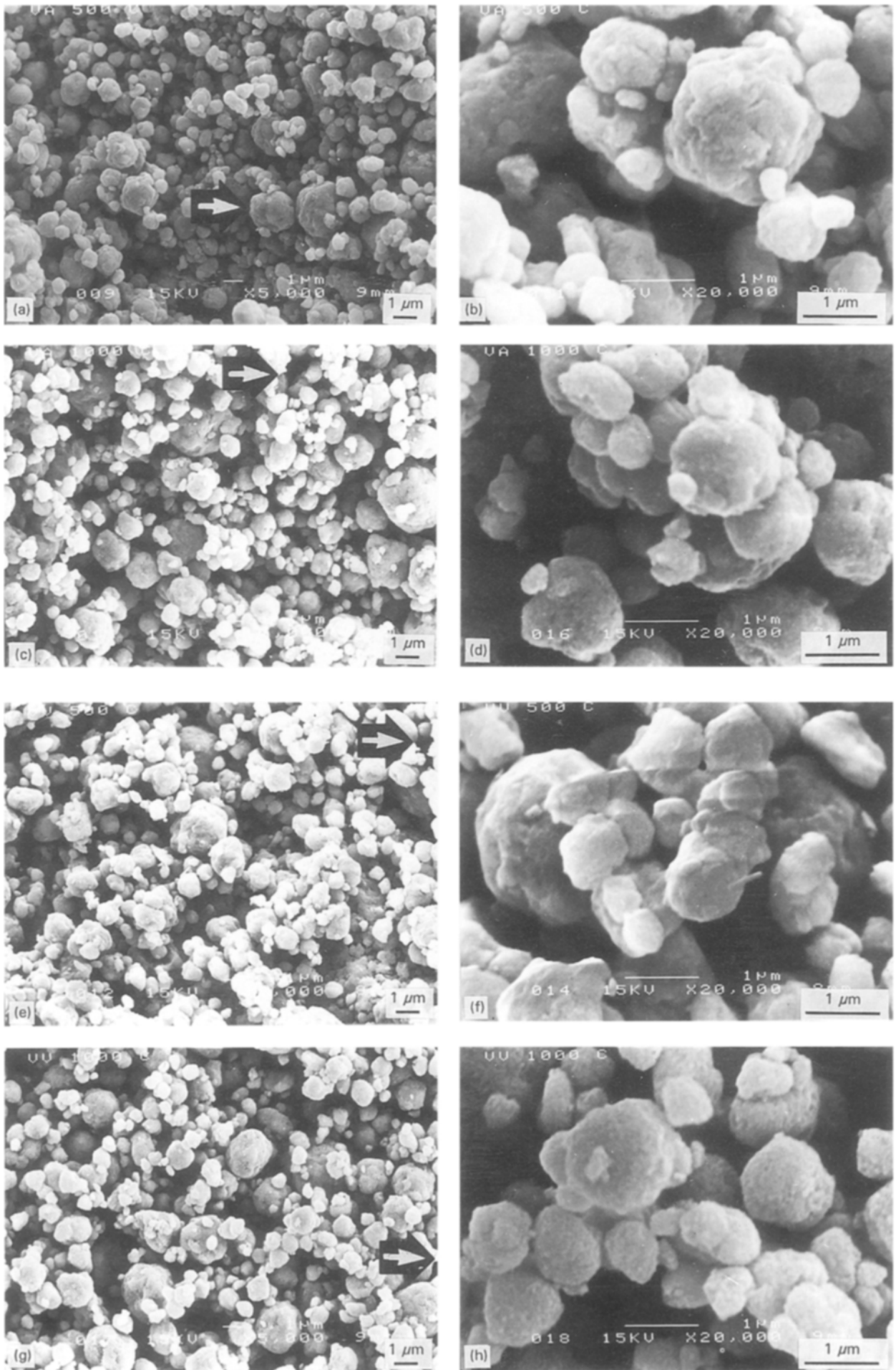


Figure 3 SEM analysis of vacuum-milled barium ferrite powder versus annealing temperature ((a, b, e, f) 773 and (c, d, g, h) 1273 K) performed in air (A) and vacuum (V). (a, b) VA773, (c, d) VA1273 (e, f) VV773, (g, h) VV1273.

annealed at 773 K the thermal activation energy is insufficient to break clusters into a separate particle dispersion and some of the agglomerates are still visible. For samples AA773 and AA1273 (cf. Fig. 2b and d) the average particle size of air-annealed powders has a tendency to decrease with annealing temperature. The scanning electron micrographs of vacuum-annealed powders AV773 and AV1273 are different from the above. Both samples show larger particle clusters with spherical shape and size in the range of 1–3 μm . In material annealed at higher temperature, small crystalline grains in the clustered particles are more evident. These have irregular shape and size in the range 0.1–0.5 μm (cf. Fig. 2f and h). At the present moment the problem of stability of particle aggregates visible in Fig. 2h for vacuum-annealed powder AV1273 and fine particle dispersion observed for AA1273 sample (Fig. 2d), cannot be answered and will be discussed below with the thermal analysis results.

Scanning electron micrographs of V1000 powder after heat treatment, presented in Fig. 3, show that the morphology of powder particles is very stable. Individual particle shape was found to be insensitive to annealing temperature and atmosphere. The particles remain near spherical with an irregular surface. Only for VV1273 sample was the particle surface found to be slightly rougher than for other samples.

3.2. XRD

X-ray diffraction patterns of as-prepared powders are presented in Figs 4a and 5a. The XRD pattern of the sample milled for 1000 h in air does allow a semi-quantitative analysis of the discernible peaks. In particular, the (107) – 37.5°, (114) – 39.8°, (205) – 47.16° and (206) – 49.7° reflections of hexagonal barium ferrite can be indexed along with the following dominant lines of the haematite, $\alpha\text{-Fe}_2\text{O}_3$, structure: (012) – 28.1°, (104) – 38.7°, (110) – 41.6°, (113) – 47.8°, (024) – 58.2° and (116) – 63.7°. In Figs 4 and 5, haematite and barium ferrite peaks are denoted by F and B, respectively. Given the compositional make-up of ferrimagnetic barium ferrite ($\text{BaO} \cdot 6\text{Fe}_2\text{O}_3$), the structure of the paramagnetic $\alpha\text{-Fe}_2\text{O}_3$ stable at room temperature, and the resistance of this simple oxide to extended dry or wet ball-milling in air [2], this partial decomposition of $\text{BaFe}_{12}\text{O}_{19}$ to $\alpha\text{-Fe}_2\text{O}_3$ and BaO (the last one undetected by XRD because of its low concentration and/or disordered state) on ball-milling in air is not unlikely. Indeed, the most intense barium ferrite XRD reflection $2\theta_{107} = 37.5^\circ$ is replaced by the strongest line for haematite $2\theta_{104} = 38.7^\circ$. Comparing the above with the XRD pattern of a vacuum sample milled for 1000 h, a weak tendency for the onset of new peaks was found. The material can be characterized as a highly disordered form. By employing an XRD fitting programme with a Gaussian line shape to data from Fig. 5a it was found that the broad feature is centered and has full width at half height: $2\theta = 36.4^\circ \pm 0.3$ and $\Delta 2\theta = 10.4^\circ \pm 0.5^\circ$, respectively. We attribute this effect to mechanically induced

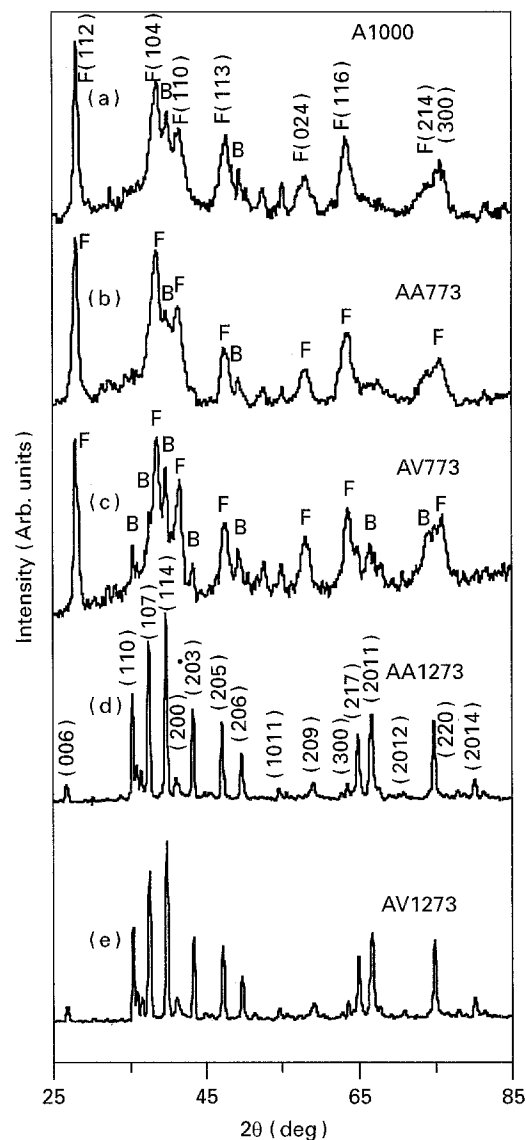


Figure 4 XRD pattern evolution of the 1000 h air-milled $\text{BaFe}_{12}\text{O}_{19}$ powder for different annealing conditions. Some of the main XRD peaks are indexed by short notation: F, Fe_2O_3 ; B, $\text{BaFe}_{12}\text{O}_{19}$. XRD pattern (d) has all the barium ferrite indexes.

structure deformations (disordering) of vacuum ball-milled material. However, in addition to this, broad XRD peaks characteristic of the haematite phase can be found in the diffraction pattern. It was concluded recently [1], that for air-milled powder the structural decomposition of barium ferrite is due to high oxygen-gas adsorption on the fine particle surface, but for vacuum-milled powder this process was found to be much slower.

By application of annealing at two temperatures, 773 and 1273 K for 4 h in air and vacuum, it was possible to find information relating recrystallization, or as used above, the phase restoration in milled powders. Both XRD and DSC thermal analysis experiments were performed on annealed samples. To characterize the results obtained, we can assume that after 4 h annealing at 1273 K, disregarding air pressure, the results are the same and the XRD patterns show perfect barium ferrite structure (schematically indexed in Fig. 4d). However, at this point we can find no explanation why the $\theta_{114} = 39.8^\circ$ line has higher

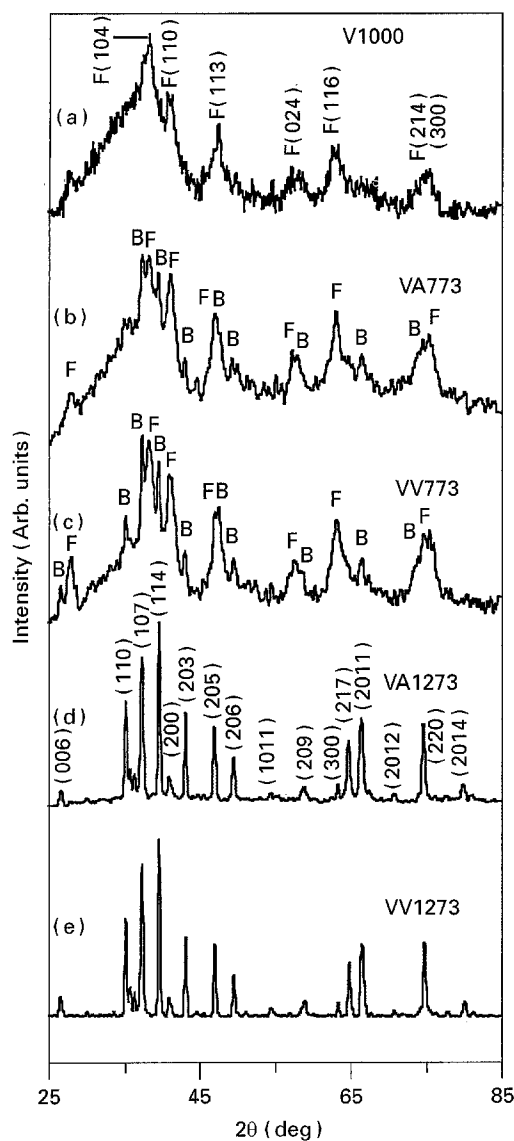


Figure 5 XRD pattern evolution of the 1000 h vacuum-milled $\text{BaFe}_{12}\text{O}_{19}$ powder for different annealing conditions. Some of the main XRD peaks are indexed by short notation: F, Fe_2O_3 ; B, $\text{BaFe}_{12}\text{O}_{19}$. XRD pattern (d) has all the barium ferrite indexes.

intensity than the $\theta_{107} = 37.7^\circ$ line, as expected, when we compare with tabulated data [4]. From other experiments with ball milling of barium ferrite powders, we found that this feature is characteristic and uninfluenced by dry or wet milling [5]. Additionally, it was concluded that no other phase can be found and the resulting powder is high-purity barium ferrite.

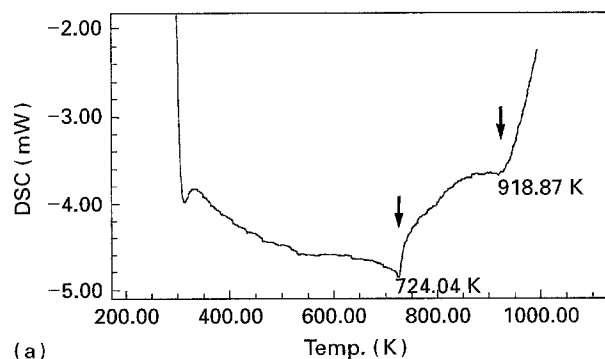
A more complex situation was found for powders annealed at lower temperature (773 K). There are some visible changes in powder structure showing the relation between multiphase composition. In a qualitative way we can describe the influence of air pressure during annealing on the barium ferrite–haematite composition ratio. As a main result we note that annealing in air further promotes the decomposition process but annealing in vacuum has the opposite effect and barium ferrite ordered-phase restoration occurs. From XRD patterns for both samples presented in Figs 4b and 5b, a decrease in the intensity of the barium ferrite characteristic peaks is observed. In this way we deduce the decreasing amount of ferrite phase.

This effect is most visible for air-milled powder. For a vacuum-milled sample, an additional process was assumed to occur, where part of the disordered barium ferrite phase (broad lines in the XRD pattern) transforms into the crystalline form and the most intense XRD peaks (107), (114), (203) and (2011) can be indexed (cf. Fig. 5b). On the other hand, for powders annealed in vacuum, the opposite situation was found. Comparing XRD peak intensity for barium ferrite and haematite, an increase in the relative composition ratio was found and the barium ferrite phase is very visible. The broad feature in the XRD pattern of vacuum-milled and vacuum-annealed powder has a tendency to disappear and the formation of ordered ferrite phase was observed to a higher degree in this powder than in an air-annealed sample (cf. Fig. 5c and b). Furthermore, both patterns in Figs 4c and 5c are more similar to each other than patterns for air-annealed powders in Figs 4b and 5b. We assume that larger and more structurally disordered particles of vacuum-milled powder are less influenced by an air atmosphere during annealing, and the observed XRD patterns changes (cf. Fig. 5b and c) have a mainly internal nature rather than external.

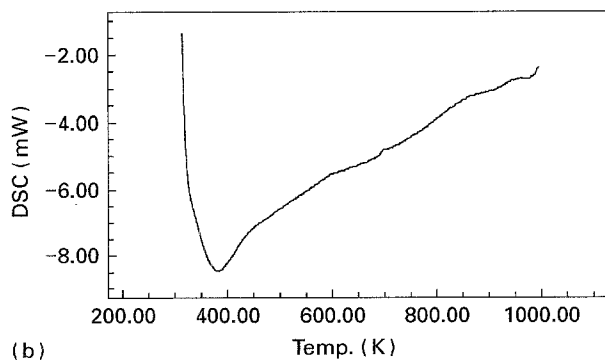
3.3. DSC and TG analysis

3.3.1. As-milled powders

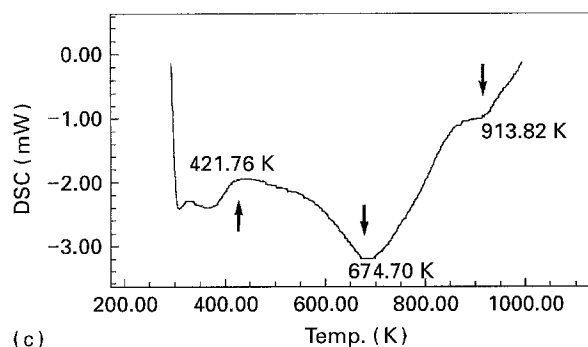
Results obtained from DSC for milled powders compared with pre-milled material are presented in Fig. 6. The DSC scan for the pre-milled ferrite powder shows a characteristic sharp endothermic peak at $T_c = 727$ K. This temperature is assigned to the ferri-paramagnetic transition Curie temperature for barium ferrite. The second characteristic feature in a temperature range around 930 K can be related to the existence of weak ferromagnetism in spinel blocks of the barium ferrite crystal structure (observed normally for $\alpha\text{-Fe}_2\text{O}_3$ crystals for temperatures up to $T_N = 955$ K). DSC scans for as-milled powders show remarkable differences, however; these results are in good agreement with XRD data. The DSC curve for powder milled in a vacuum, Fig. 6c, has all the characteristic features observed for pre-milled material and powder milled in air. The minimum of the broad endothermic peak assigned to the Curie temperature, $T_c = 683$ K, was found, 10% below the value of bulk barium ferrite. An additional high-temperature curve bend ~ 910 K is also observed. However, some additional changes are visible in the low-temperature range ~ 370 K, a feature characteristic for powder milled in air (cf. Fig. 6c and b). By using XRD data in the explanation of DSC results, we conclude that the air-milled sample is more compositionally homogeneous (paramagnetic $\alpha\text{-Fe}_2\text{O}_3$ phase with minimal content of barium ferrite), than vacuum-milled powder where two phases are clearly visible: the main disordered barium ferrite contaminated by the reduction product, haematite. Furthermore, results of thermogravimetric analysis (TGA) of powders milled in air and vacuum show in a direct way the composition difference between both samples. The observed weight decrease for air-milled powder in the temperature



(a)



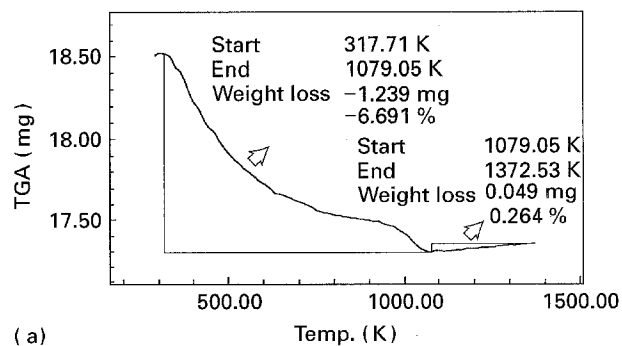
(b)



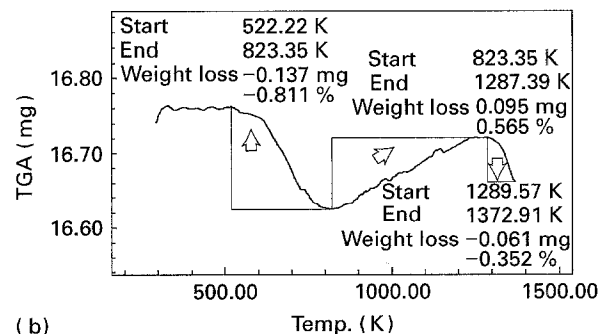
(c)

Figure 6 DSC results for as-milled powders: (a) pre-milled material, (b) A1000 and (c) V1000. All curves were recorded with an argon flow rate of 50 ml min^{-1} , temperature programme rate 30 K min^{-1} and sample weight: (a) 24.77 mg, (b) 19.75 mg and (c) 17.01 mg.

range 330–1070 K has a significantly high value of 6.62 wt %, and as we found recently [1], oxygen loss (desorption) is mainly responsible for this. The final weight decrease in the temperature range 920–1070 K observed in the TGA scan, can be attributed to barium ferrite recrystallization. The number of oxygen molecules, O_2 , per one crystallographic barium ferrite unit cell ($2 \times \text{BaFe}_{12}\text{O}_{19}$) at room temperature can be obtained by calculation from the weight loss, and was found to be ~ 1.2 . This result shows that statistically nearly one additional oxygen atom is connected to one barium ferrite molecule. At the present moment it is difficult to discuss this “superoxide formation” problem in detail, because of the unknown nature of the bonding. A TGA scan for vacuum-milled material in Fig. 7b shows a different thermal characteristic weight loss factor, with ten times lower magnitude. Weight loss can be observed in a narrow range of temperature, 570–820 K. Subsequently, weight increases over a much broader temperature range,



(a)



(b)

Figure 7 TGA scan for as-milled powders: (a) A1000 and (b) V1000. Both curves were recorded with an argon flow rate of 80 ml min^{-1} and temperature programme rate 30 K min^{-1} .

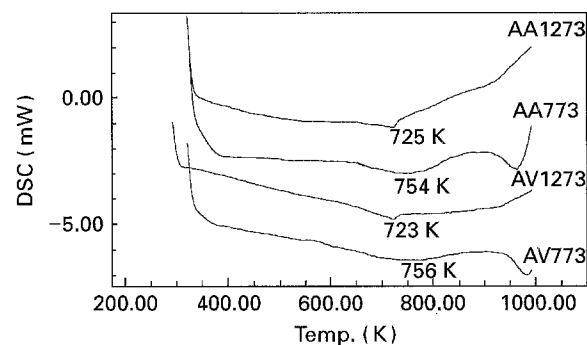


Figure 8 DSC results for annealed air-milled powders. All curves were recorded with an argon flow rate of 50 ml min^{-1} , temperature programme rate 15 K min^{-1} and sample weight in the $22 \pm 2 \text{ mg}$ range.

820–1270 K. We assume that trace-gas desorption occurs up to 820 K as the nanocrystalline structure is under thermal stress relaxation, and then barium ferrite crystal grain growth requires oxygen (argon used in TGA experiments has oxygen contamination) to fill up its vacancies. The same effect is visible for sample A1000 in the high-temperature range (cf. Fig. 7a). During thermal treatment of samples A1000 and V1000, a regrowth of grains of the ordered phase occurs. For the last sample it can be more accurately described as a transformation process between nanostructured (or disordered and partly decomposed) material and ordered crystalline phase.

3.3.2. Annealed powders

DSC curves of annealed powders are presented in Figs 8 and 9. For all powders annealed at 1273 K, thermal

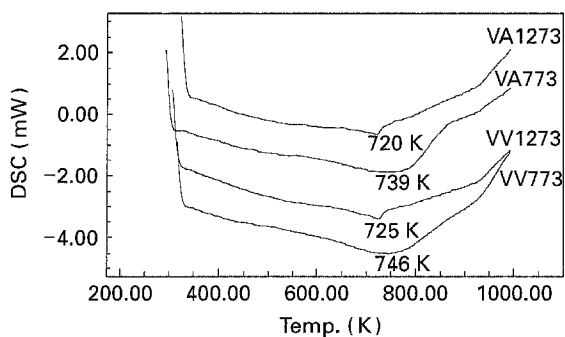


Figure 9 DSC results for annealed vacuum-milled powders. All curves were recorded with an argon flow rate of 50 ml min^{-1} , temperature programme rate 15 K min^{-1} and sample weight in $18 \pm 2 \text{ mg}$ range.

analysis shows the same features visible on the DSC curves. The only observed difference was found in the value of the minimum temperature. As described above, this temperature minimum specifies directly the magnetic Curie temperature, $T_c = 723 \pm 5 \text{ K}$, a characteristic value of barium ferrite. We note that the observed difference is minimal. A more complicated situation was obtained for powders annealed at 773 K where for all DSC curves, characteristic features are broader. These results are in good agreement with XRD patterns (Figs 4b, c and 5b, c) where the existence of a disordered phase contribution is clearly visible. Additionally, we found a similarity between DSC results for samples annealed at 773 K, and the DSC scan recorded for the V1000 sample (cf. Fig. 6c). This can be well understood if we take into consideration the TGA results presented above. We assume that at 773 K, most of the oxygen atoms are removed from the annealed powder, the process of barium ferrite phase restoration starts and in this situation thermal analysis results are similar. An additional high-temperature minimum was observed for two samples, AA773 and AV773. The same behaviour was already observed in the TGA plot (Fig. 7a) which was found to be characteristic only for air-milled material. Lack of an obvious dependence on annealing conditions (air or vacuum) shows that effect has an intrinsic nature. We assume that in the 920–1020 K temperature range, the final oxygen discharge from the powder occurs. This effect is only characteristic for air-milled material and non-existent for vacuum-milled samples.

4. Conclusions

A thermally activated crystalline phase restoration process in disordered $\text{BaFe}_{12}\text{O}_{19}$ ferrite powders, prepared by 1000 h ball milling in air or vacuum, was

investigated. Air-milled material has to form a gas-saturated disordered structure (superoxide) and to transform into simple oxides (reduction process through oxygen-saturated disordered phase) contrary to the vacuum-milled powder where a highly disordered phase occurs. As-milled powders have a different morphology. Heat treatment was performed on air- or vacuum-milled samples at two temperatures (773 and 1273 K) for 4 h, both in air and vacuum. The annealing process produces a crystalline barium ferrite phase with interesting magnetic properties (typical magnetic saturation with extremely high coercivity, depending strongly on the temperature and air pressure during the annealing process), but in the present paper, only structural transformations were analysed.

1. Morphological examination shows that particle size and distribution are less influenced by different conditions during annealing (temperature and gas pressure), as can be expected assuming that typical recrystallization processes will occur. Contrary to the normal recrystallization process, crystalline phase restoration in ball-milled barium ferrite powder has a different nature. The size distribution remains in the same range and minimal changes in roughness are visible on the particle surface.

2. XRD analysis shows that increase of the annealing temperature to 1273 K has a remarkable effect on powder crystallographic structure. Air pressure during annealing has no influence on structural and thermal properties. However, the structure of samples annealed at a lower temperature (773 K) depends on air pressure during annealing and shows a multiphase structure (haematite, barium ferrite and disordered phase), while those prepared at 1273 K are homogeneous, i.e. single-phase hexagonal barium ferrite.

Acknowledgement

This study was partly supported by a grant from IAS-Australian Universities Collaboration Scheme IAS9322.

References

1. W. A. KACZMAREK, *Materials Science Forum* **179–181** (1995) 313.
2. W. A. KACZMAREK and B. W. NINHAM, *IEEE Trans. Magn.* **MAG-30** (1994) 732.
3. J. S. REED, "Introduction to the Principles of Ceramic Processing" (Wiley-Interscience, New York, 1988) p. 25.
4. PDF-2 database file no: 27-1029, JCPDS-ICDD (1992).
5. W. A. KACZMAREK and B. W. NINHAM, *Mater. Chem. Phys.* **40** (1995) 21.

Received 1 June 1994

and accepted 22 June 1995